Schweizerische Eidgenossenschaft
Confédération suisse
Confederazione Svizzera
Confederaziun svizra

Federal Department of the Environment,
Transport, Energy and Communications DETEC

Swiss Federal Office of Energy
Energy Research and Cleantech

Final report from 27 August 2026

ALISA

Advanced Lithium-Sulfur Batteries with Ultramicroporous Carbons



Publisher:
Swiss Federal Office of Energy SFOE
Energy Research and Cleantech
CH-3003 Berne
www.energy-research.ch

Agent:
ETH Zürich
Gloriastrasse 35
8092 Zürich
www.ethz.ch

Authors:
Ayca Senol, ETH Zürich, ayca.senol@ife.ee.ethz.ch
Christian Prehal, ETH Zürich (since 07/23 University of Salzburg, Austria), christian.prehal@plus.ac.at
Vanessa Wood, ETH Zürich, vwood@ethz.ch

SFOE project coordinators:
Philipp Müller, philipp.mueller@bfe.admin.ch
Stefan Oberholzer, stefan.oberholzer@bfe.admin.ch

SFOE contract number: SI/502458-01

The authors bear the entire responsibility for the content of this report and for the conclusions drawn therefrom.

Summary

The ALISA project (Advanced Lithium–Sulfur batteries with ultramicroporous carbons) addressed one of the key challenges in developing next-generation rechargeable batteries: enabling high-energy, sustainable, and safe lithium–sulfur (Li–S) cells. Unlike conventional lithium-ion technology, Li–S batteries rely on abundant and low-cost sulfur, offering the potential for significantly higher energy densities and reduced environmental impact.

Sulfur cathodes and electrolytes were optimized through innovative infiltration methods and systematic benchmarking of carbonate-based electrolytes. *Operando* and *ex situ* characterization techniques such as SAXS/SANS, XRD, XPS, and cryo-TEM provided unprecedented insight into how sulfur converts inside nanopores and how the cathode–electrolyte interphase (CEI) forms and evolves during cycling.

ALISA successfully demonstrated that Li–S batteries with novel porous carbons and optimized carbonate electrolytes can achieve stable, long-life operation at the laboratory scale. The project generated new mechanistic understanding of sulfur conversion and CEI chemistry, delivered a wide portfolio of advanced carbon materials, and highlighted both opportunities and challenges for scaling towards practical devices. The outcomes provide a strong foundation for future European research and industrial innovation in post-lithium battery technologies.

Zusammenfassung

Das ALISA-Projekt (Fortschrittliche Lithium-Schwefel-Batterien mit ultramikroporösen Kohlenstoffen) befasste sich mit einer der zentralen Herausforderungen bei der Entwicklung wiederaufladbarer Batterien der nächsten Generation: der Realisierung energiereicher, nachhaltiger und sicherer Lithium-Schwefel-Zellen (Li–S). Im Gegensatz zur konventionellen Lithium-Ionen-Technologie basieren Li–S-Batterien auf reichlich verfügbarem und kostengünstigem Schwefel und bieten damit das Potenzial für deutlich höhere Energiedichten und geringere Umweltauswirkungen.

Schwefelkathoden und Elektrolyte wurden mithilfe innovativer Infiltrationsmethoden und einer systematischen vergleichenden Bewertung carbonatbasierter Elektrolyte optimiert. *Operando*- und *Ex situ*-Charakterisierungsmethoden wie SAXS/SANS, XRD, XPS und Kryo-TEM ermöglichten bisher unerreichte Einblicke in die Umwandlung von Schwefel in Nanoporen sowie in die Bildung und Entwicklung der Kathoden-Elektrolyt-Grenzphase (CEI) während des Zyklierens.

ALISA zeigte erfolgreich, dass Li–S-Batterien mit neuartigen porösen Kohlenstoffen und optimierten carbonatbasierten Elektrolyten im Labormaßstab einen stabilen und langlebigen Betrieb erreichen können. Das Projekt lieferte neue mechanistische Erkenntnisse zur Schwefelumwandlung und CEI-Chemie, entwickelte ein breites Portfolio fortschrittlicher Kohlenstoffmaterialien und zeigte sowohl Chancen als auch Herausforderungen bei der Skalierung hin zu praxistauglichen Anwendungen auf. Die Ergebnisse bilden eine solide Grundlage für zukünftige europäische Forschung und industrielle Innovation im Bereich der Post-Lithium-Batterietechnologien.

Résumé

Le projet ALISA (Batteries lithium-soufre avancées à base de carbones ultramicroporeux) s'est attaqué à l'un des principaux défis liés au développement des batteries rechargeables de prochaine génération: permettre la réalisation de cellules lithium-soufre (Li–S) à haute densité énergétique, durables et sûres. Contrairement à la technologie lithium-ion conventionnelle, les batteries Li–S reposent sur le soufre, un

matériau abondant et peu coûteux, et offrent ainsi la possibilité d'atteindre des densités énergétiques nettement supérieures tout en réduisant leur impact environnemental.

Les cathodes soufrées et les électrolytes ont été optimisés grâce à des méthodes d'infiltration innovantes et à une évaluation comparative systématique des électrolytes à base de carbonates. Des techniques de caractérisation *operando* et *ex situ*, telles que la SAXS/SANS, la XRD, la XPS et la cryo-TEM, ont fourni des informations sans précédent sur la transformation du soufre dans les nanopores ainsi que sur la formation et l'évolution de l'interphase cathode-électrolyte (CEI) au cours du cyclage.

ALISA a démontré avec succès que les batteries Li–S utilisant de nouveaux carbones poreux et des électrolytes carbonatés optimisés peuvent fonctionner de manière stable et durable à l'échelle du laboratoire. Le projet a permis d'acquérir une nouvelle compréhension mécanistique de la transformation du soufre et de la chimie de la CEI, de développer un large éventail de matériaux carbonés avancés et de mettre en évidence les possibilités et les défis liés au passage à l'échelle vers des dispositifs pratiques. Ces résultats constituent une base solide pour les futures recherches européennes et les innovations industrielles dans le domaine des technologies de batteries post-lithium.

Main findings («Take-Home Messages»)

- ALISA developed a broad portfolio of tailored porous carbons, including biomass-derived materials, with controlled ultramicroporosity and surface chemistry for improved sulfur confinement.
- Optimized sulfur infiltration and carbonate-based electrolytes enabled reversible solid-state sulfur conversion and stable laboratory-scale cycling, including more than 300 cycles with selected biocarbon cathodes.
- Advanced *operando* and *ex situ* characterization clarified sulfur conversion inside nanopores and the formation of the cathode–electrolyte interphase, while data-driven modelling accelerated SAXS/SANS analysis by approximately 1000 times.
- By advancing sustainable battery materials, training researchers, and identifying the remaining scale-up challenges, ALISA strengthened the European and Swiss knowledge base for future energy-storage technologies. The project supports Swiss energy-policy objectives by promoting innovation in resource-efficient batteries based on abundant sulfur and carbon materials.

The ALISA project (Advanced Lithium–Sulfur Batteries with Ultramicroporous Carbons) successfully explored, designed, and validated novel carbon hosts, electrolytes, and characterization approaches for next-generation Li–S batteries. Over its 36-month duration from September 2022 to August 2025, the consortium generated fundamental scientific knowledge, demonstrated new material architectures, and identified important challenges for industrialization.

A broad library of porous carbons was synthesized and optimized, including carbide-derived carbons, novolac-derived carbons, Porocarbs, carbon spherogels, and biomass-derived carbons such as olive-pomace-based CB700. Controlled pore sizes between 0.7 and 1.8 nm and heteroatom functionalization with nitrogen and phosphorus enabled the surface chemistry and sulfur confinement properties of these materials to be tailored systematically.

A robust sulfur-infiltration protocol was established, and systematic benchmarking identified carbonat-based electrolytes with high FEC content as the most stable systems for reversible solid-state sulfur conversion. High-sulfur-loading cathodes containing NPC and Porocarb materials achieved stable cycling for more than 50 cycles, while selected biocarbon cathodes retained capacities of approximately 850 mAh g^{-1} for more than 300 cycles. A pouch-cell prototype was also fabricated, demonstrating the feasibility of transferring the developed concepts to a larger format while revealing remaining challenges related to lithium-metal stability and electrolyte distribution.

Operando SAXS/SANS, XRD, XPS, and cryo-TEM provided new mechanistic insights into sulfur conversion and cathode–electrolyte interphase formation. The results confirmed solid-state sulfur conversion within micropores and showed that CEI chemistry strongly depends on the electrolyte and applied voltage. Carbonate-based electrolytes formed comparatively robust, inorganic-rich interphases, whereas ether-based electrolytes resulted in less stable, polysulfide-dominated interphases. CNN-based SAXS/SANS modelling accelerated data analysis by approximately 1000 times, enabling substantially faster processing of complex operando datasets.

The project also achieved extensive scientific dissemination and researcher training. Its results contributed to more than ten high-impact publications, presentations at major international conferences, and an open-access Zenodo repository. Despite the withdrawal of one industrial partner during the project, the consortium successfully redistributed the affected tasks without compromising overall progress.

Overall, ALISA established important structure–property relationships for advanced porous carbons, clarified the mechanisms governing sulfur conversion and CEI formation, and identified promising materials and electrolytes for future development. At the same time, it defined critical bottlenecks for practical implementation, particularly pouch-cell scale-up and lithium-metal stability. By advancing battery technologies based on abundant sulfur and tailored carbon materials, the project contributes to the research and innovation needed for more sustainable energy storage and supports the broader objectives of Switzerland’s Energy Strategy 2050.

Contents

Summary ... **3**
Zusammenfassung ... **3**
Résumé ... **3**
Main findings («Take-Home Messages») ... **4**
Contents ... **6**
List of abbreviations ... **8**
1 Introduction ... **9**
1.1 Context and motivation ... 9
1.2 Project objectives ... 11
2 Approach, method, results and discussion ... **12**
3 Conclusions and outlook ... **23**
4 National and international cooperation ... **24**
5 Publications and other communications ... **25**
6 References ... **25**
7 Project progress (confidential) ... **26**
8 Data management plan and open access/data/model strategy (confidential) ... **28**

List of abbreviations

SFOE	Swiss Federal Office of Energy

1 Introduction

1.1 Context and motivation

Lithium-sulfur (Li-S) batteries are considered a promising next-generation energy storage technology due to the high theoretical specific energy (1672 mAh g^{-1}) as well as the low cost and natural abundance of sulfur (1). In combination with a metallic lithium anode (high specific capacity of 3860 mAh g^{-1} and low electrode potential of -3.04 V vs. SHE), they are widely regarded as achieving gravimetric energy density targets beyond the limits of today's lithium-ion technology (2). Conventional liquid-electrolyte Li-S batteries consist of a carbon/sulfur composite positive electrode (cathode), an organic, often ether-based, liquid electrolyte such as 1 M LiTFSI in Bis(2-methoxyethyl)ether (diglyme), and a lithium metal negative electrode (anode) (3).

During discharge, lithium is oxidized at the lithium metal anode, releasing Li^+ ions that migrate through the electrolyte toward the cathode. At the cathode, sulfur is reduced to lithium sulfide via a multistep electrochemical reaction involving dissolved lithium polysulfides (Figure 1a). During charging, the reverse reactions occur, oxidizing lithium sulfide back to elemental sulfur (4).

The characteristic discharge and charge curves of common Li-S batteries with solvating electrolytes exhibit two distinct voltage plateaus. The first plateau, located at approximately 2.3 - 2.4 V vs. Li/Li^+, is associated with the reduction of elemental sulfur to higher-order polysulfides such as Li_2S_8. The second plateau, around 2.0 - 2.1 V vs. Li/Li^+, corresponds to the further reduction of lower-order polysulfides (e.g., Li_2S_6, Li_2S_4) to insoluble Li_2S. During charging, these processes occur in reverse order (Figure 1b). Both sulfur and lithium sulfide are electronically and ionically insulating, which precludes a direct solid-state conversion with micrometer-sized sulfur crystallites and necessitates a solution-mediated reaction pathway involving dissolved polysulfides. This solid-liquid-solid conversion mechanism is fundamentally different from the intercalation-based charge storage mechanism in conventional lithium-ion batteries and gives rise to challenges intrinsic to Li-S chemistry (5).

While specific energies are high in theory, in a practical cell, we need a minimum electrolyte amount to promote polysulfide dissolution and enable electrochemical conversion. The high electrolyte amount destroys the specific energy of the entire cell, despite the high theoretical capacity of the active material. The dissolved polysulfides also lead to capacity fading and poor cycle life, as they can diffuse to the anode, where they react irreversibly. Shuttling polysulfides between the cathode and anode, which are reversibly oxidized and reduced, can lead to fast self-discharge. Finally, the rate performance and power densities of Li-S batteries are low due to slow conversion kinetics. This might be related to poor charge transfer rates and the insulating nature of the solid active materials, S and Li_2S.

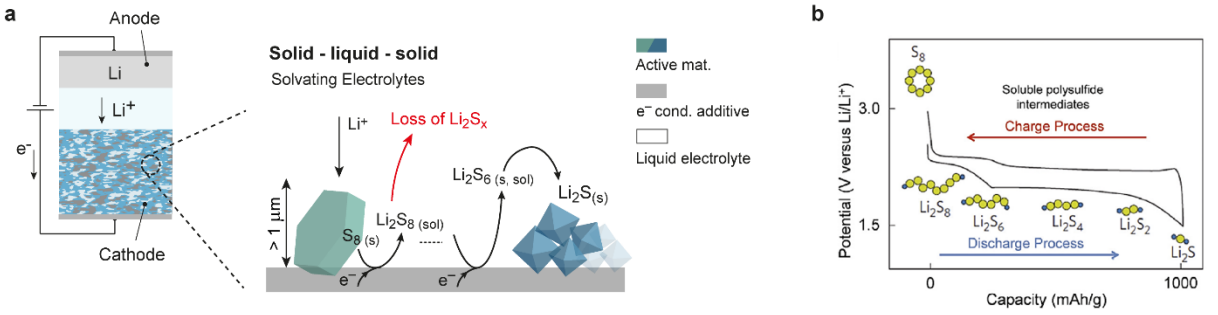


Figure 1. (a) Schematics of a Li-S battery cell stack and the common solid-liquid-solid discharge process in a Li-S battery with solvating electrolytes (often ether-based). (b), Common voltage profile during galvanostatic charge/discharge of a Li-S battery with solvating electrolyte. The profile shows two distinct plateaus at 2.4 V vs. Li/Li+ and 2.15 V vs Li/Li+. Reproduced with permission from (4).

Current State of the Technology and Applications

The lightweight nature of sulfur (density = 2.07 g cm^{-3}) and its high theoretical specific capacity of 1672 mAh g^{-1} make Li-S batteries particularly attractive for applications where gravimetric energy density is critical. At the cell level, Li-S batteries are projected to achieve specific energies of up to ~400 Wh kg^{-1}, significantly exceeding the ~240-300 Wh kg^{-1} of state-of-the-art lithium-ion batteries (6). As a result, Li-S batteries are considered especially promising for mobility applications where battery mass is a limiting factor, such as high-altitude pseudo-satellites, drones/UAVs, electric aviation, and heavy-duty electric transportation (Figure 2a) (7,8). In such applications, reductions in battery mass directly translate into increased payload, extended range, or improved overall system efficiency (7). In parallel, the sulfur cathode offers a materials-sustainability narrative (reduced reliance on Ni/Co-containing cathodes), which is increasingly relevant for supply-chain resilience and geopolitical considerations.

However, practical Li-S batteries can, at the moment, hardly outperform current Li-ion technology (9). Although pouch-cell type prototype Li-S cells with specific energies approaching 400 Wh kg^{-1} have been reported (6,10), these high-energy demonstrations typically exhibit poor cycle life (Figure 2b). In such cases, cycle life is often limited to fewer than 100 cycles (6). This rapid degradation is largely attributed to parasitic reactions at the lithium metal anode: at the ultralow E/S ratios required to achieve high gravimetric energy density, continuous and poorly controlled SEI formation consumes much of the electrolyte after only a few cycles (11). In addition, Li-S batteries commonly suffer from low rate capability, with practical charge and discharge rates frequently restricted to below 0.2 C, which limits their suitability for many applications (7). High specific power of up to 500 W kg^{-1} typically results in poor specific energies not higher than approximately 200 Wh kg^{-1} (Figure 2c) (10). While sulfur itself is inexpensive, current cost estimates for Li-S batteries still span a wide range, approximately 36-130 USD kWh^{-1}, reflecting uncertainties related to cell design, materials utilization, and long-term stability (7).

Li-S batteries have already reached performance levels in terms of specific energy that make them commercially relevant for niche applications, despite their remaining limitations in cycle life and power density (e.g. light-weight drones). For applications that tolerate moderate cycle life and low C-rates, Li-S technology has begun to demonstrate practical viability. Because of that, Li-S spans a wide range of technology readiness levels (TRLs), from TRL ~2-4 (new electrolytes/conversion concepts at coin-cell level) to TRL ~5-7 for selected pouch-cell prototypes and niche deployments (7).

Manufacturing-oriented reviews (12) emphasize that, although some process steps are compatible with Li-ion production, dedicated process development is required for Li-S systems. Cathode fabrication can follow conventional slurry mixing and coating routes, but higher carbon fractions and adapted binder systems are typically necessary to maintain electronic percolation and accommodate volume changes. At the same time, achieving high sulfur loading while minimizing the electrolyte-to-sulfur (E/S) ratio remains critical for competitive energy density. Given the sensitivity of Li_2S, an absolute minimum water and oxygen content in Li-S batteries is essential. The lithium-metal anode introduces more substantial deviations from Li-ion manufacturing. Thin lithium foils (<25 µm) are desirable for high energy density, yet handling and processing require extremely low moisture levels and often inert environments. Slitting, stacking, and lamination differ significantly from graphite-based production and pose additional engineering challenges. Pouch-cell formats currently dominate due to their compatibility with lithium metal and volume changes (11).

In parallel to academic advances, industrial interest in Li-S batteries has increased over the past decade, with multiple companies pursuing different technical pathways toward commercialization. Early developers such as Oxis Energy focused on ether-based Li-S systems targeting aviation and high-altitude pseudo-satellite applications, before entering administration in 2021; substantial portions of Oxis's intellectual property were subsequently acquired by Gelion, consolidating prior Li-S developments within a new industrial framework (13). More recently, companies like Lyten, Zeta Energy (in collaboration with Stellantis), and Theion have announced Li-S development programs emphasizing different approaches, ranging from C/S composite cathodes, electrolyte engineering, to sulfur confinement strategies and lithium-metal stabilization (13–16). Target applications vary from lightweight drones and aerospace systems to long-term ambitions in electric mobility.

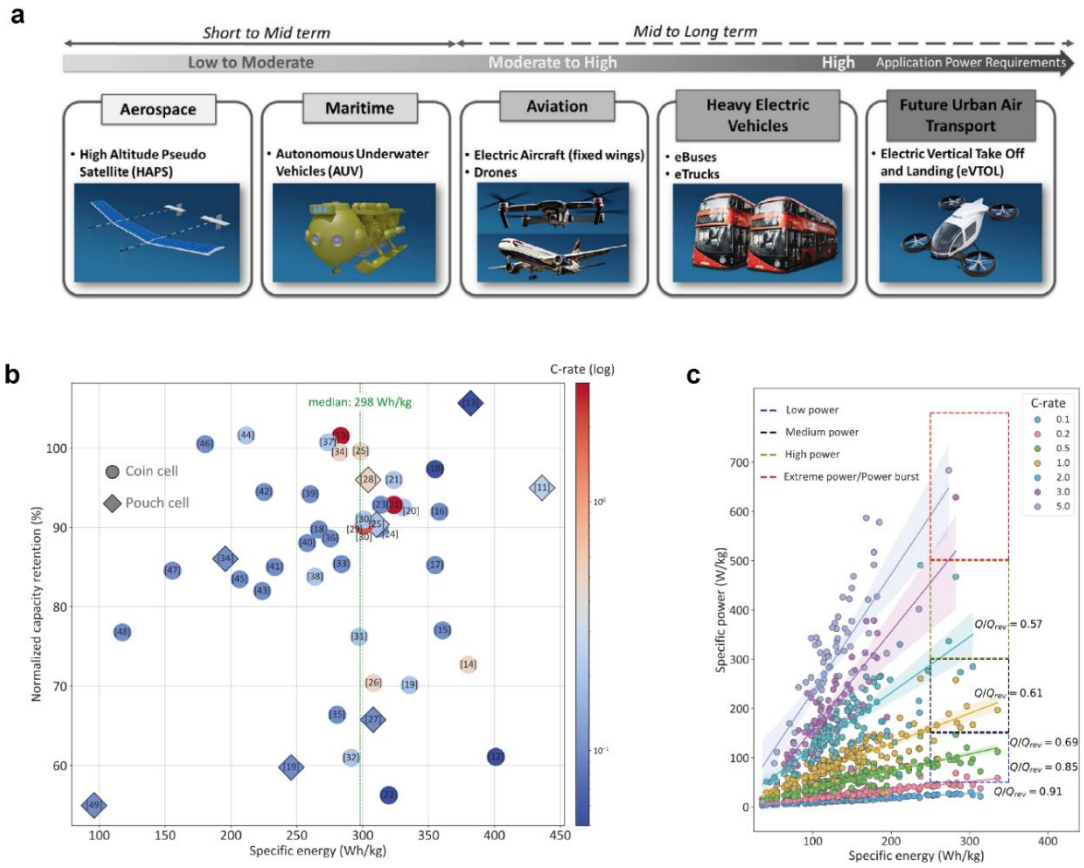


Figure 2. (a), Overview of Li-S battery applications. Reproduced with permission from (7). (b), Normalized capacity retention versus specific energy for the best performing Li-S battery prototypes demonstrated in literature. (c), Specific power versus specific energy for selected works from literature. The lower the C-rate, the lower the specific energy achieved. (a) and (b) are reproduced with permission from (10).

1.2 Project objectives

The central objective of ALISA was to develop long-cycle-life, high-capacity, and potentially low-cost lithium–sulfur (Li–S) batteries based on liquid carbonate electrolytes and ultramicroporous carbon (UMC)/sulfur composite cathodes. The battery concept relied on the confined solid-state conversion of sulfur, ultimately forming lithium sulfide (Li_2S). Ultramicropores with pore sizes below 1 nm play a decisive role in determining battery performance and lifetime. Carbonate-based electrolytes promote the formation of a cathode–electrolyte interphase (CEI) on UMC/sulfur cathodes. Unlike the solution-mediated reaction pathway typically observed with ether-based electrolytes, this interphase suppresses the formation of soluble polysulfides and enables sulfur conversion within the micropores. This mechanism can support long cycle life under lean-electrolyte conditions. Accordingly, ALISA sought to identify critical nanoscale structure–property relationships, establish rational design criteria for carbons with tailored ultramicropore and macropore architectures, and demonstrate improved performance in a prototype Li–S cell.

ETH Zürich's primary contribution to ALISA focused on establishing structure-based design criteria for carbon materials using advanced characterization methods. *Operando* small- and wide-angle X-ray scattering (SAXS/WAXS) and small-angle neutron scattering (SANS), combined with cryogenic transmission electron microscopy (cryo-TEM), were used to investigate sulfur conversion and the formation of reaction products in carbonate-based electrolytes. Electron energy-loss spectroscopy (EELS)

performed during cryo-TEM measurements further supported the identification and spatial analysis of sulfur- and lithium-containing reaction products and CEI components. Together, these complementary techniques provided structural information across multiple length scales and under both *operando* and post-mortem conditions.

These insights into sulfur conversion within ultramicroporous carbons were used to relate pore architecture and interfacial chemistry to electrochemical performance and to derive design criteria for increasing active-material loading and accessible capacity. Cryo-STEM/EELS, which is still a comparatively recent technique in battery research, represented an important element of this characterization approach because it enabled sensitive reaction products and interphases to be examined with reduced alteration. Its combination with *operando* SAXS, WAXS, and SANS substantially expanded the ability to investigate conversion mechanisms in post-lithium-ion batteries. The expertise developed at ETH Zürich through ALISA strengthened Switzerland's battery-research capabilities and contributed to the broader development of sustainable, high-capacity energy-storage technologies.

2 Approach, method, results and discussion

Approach and methodology

Small-Angle Neutron and X-Ray Scattering

Small-angle scattering (SAS), including small-angle neutron scattering (SANS) and small-angle X-ray scattering (SAXS), was used to investigate structural features of the battery materials at the nanoscale. In these techniques, a neutron or X-ray beam interacts with the sample, and the intensity scattered at small angles, typically below approximately 10°, is recorded as a function of the scattering vector. The resulting data provide information about the size, shape, orientation, internal interfaces, and spatial arrangement of nanostructures within the investigated material.

SAS offered several advantages for investigating structural changes in lithium–sulfur (Li–S) batteries. The relatively large illuminated sample volume generated a representative, volume-averaged signal from a large number of particles and nanostructures. This reduced the influence of local heterogeneities and enabled statistically meaningful changes in the overall electrode structure to be identified.

A further advantage was the compatibility of SAS with operando measurements. Structural changes could therefore be monitored while the cells were electrochemically charged and discharged. Correlating the evolution of the scattering signal with the electrochemical response provided information about changes in the carbon pore structure, sulfur distribution, and formation of discharge and charge products during cycling.

The primary focus of ALISA was the investigation of carbonate-based electrolytes combined with microporous carbon hosts. To assess the applicability of SAS to different Li–S battery concepts, three principal configurations were investigated:

- Ether-based electrolytes combined with carbon black;
- Carbonate-based electrolytes combined with microporous carbons; and

Battery cells compatible with *operando* SAXS and SANS measurements were developed or adapted for these investigations. Comparing the different battery configurations demonstrated the broader applicability of the scattering methods and supported the investigation of their respective sulfur-conversion mechanisms.

Battery-Cell Designs for Operando SAXS and SANS

Operando SAXS and SANS measurements required specially designed electrochemical cells that allowed the incident and scattered radiation to pass through the complete battery stack while maintaining electrochemical function and protecting the cell components from air and moisture.

For SAXS measurements, openings were introduced into the stainless-steel current collectors and sealed with an X-ray-transparent polymer foil, such as Kapton or Mylar. The foil provided an accessible X-ray window while maintaining the gas-tight sealing of the cell (Figure 3a).

For SANS measurements, aluminium current collectors were used instead of stainless steel because aluminium exhibits comparatively weak neutron scattering and absorption. The aluminium component could therefore function directly as the neutron window, eliminating the need for an additional window material (Figure 3b). Because lithium metal can react with aluminium, a protective copper foil was placed between the lithium-metal anode and the aluminium current collector.

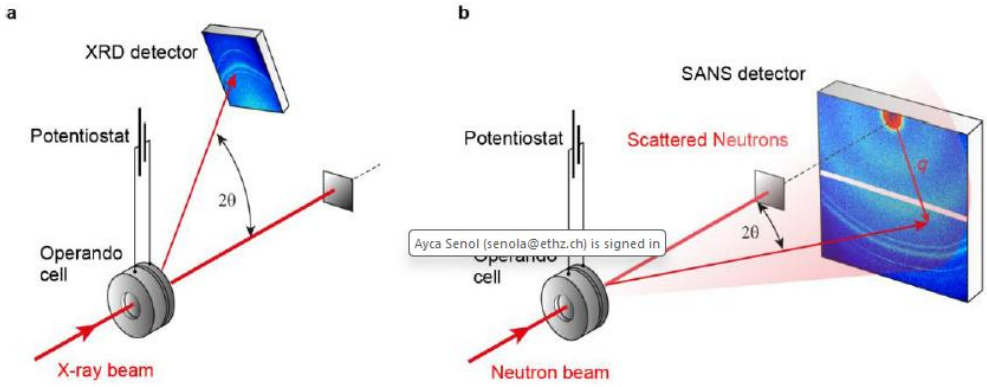


Figure 3. Sketch of the *operando* experimental set-up. (a), Set-up for *operando* X-ray diffraction (XRD). (b), Set-up for *operando* small angle neutron scattering (SANS).

Cryogenic Transmission Electron Microscopy

Cryogenic transmission electron microscopy (cryo-TEM) was used to investigate nanostructured sulfur cathodes and their electrochemical reaction products. Conventional electron-microscopy conditions present substantial challenges for Li–S battery materials because sulfur can sublime under high vacuum and electron-beam exposure, while metastable discharge products and interphases may undergo structural or chemical alteration. Maintaining the samples at cryogenic temperatures reduced these effects and enabled the sensitive phases to be examined in a state closer to that present in the electrochemical cell.

Cryogenic conditions were particularly important for chemical analysis by energy-dispersive X-ray spectroscopy (EDS) and electron energy-loss spectroscopy (EELS). In combination with TEM and scanning TEM (STEM), these techniques enabled the spatial distribution and chemical state of sulfur-containing reaction products and cathode–electrolyte interphase components to be investigated at the nanoscale. Cryo-TEM therefore complemented the volume-averaged information obtained from *operando* SAXS and SANS with localized structural and chemical information.

Cryo-FIB-SEM Sample Preparation

Preparing Li–S cathodes for cryo-TEM required a specialized workflow because lithium sulfide (Li_2S), interphase components, and other reaction products are highly sensitive to air, moisture, vacuum, and electron-beam exposure. All sample handling was therefore conducted under inert or cryogenic-vacuum conditions.

Cryogenic focused-ion-beam scanning electron microscopy (cryo-FIB-SEM) was performed at ScopeM using a Helios NanoLab 600i dual-beam microscope (FEI/Thermo Fisher Scientific). A lamella was

prepared from a non-ball-milled electrode after its first discharge for subsequent TEM, STEM, EELS, and EDS characterization. The electrode was recovered from the cell in an argon-filled glovebox with O_2 and H_2O concentrations below 0.1 ppm. Active material was gently scratched from the electrode onto carbon tape without exposure to ambient air.

The sample was transferred from the glovebox to the FIB-SEM instrument using an EM VCT100 vacuum cryo-transfer system (Leica). During cryo-FIB-SEM preparation, the stage temperature was maintained at approximately −150 °C under high-vacuum conditions at a pressure of approximately 2×10^{-6} mbar.

A particle measuring approximately 15 µm in each dimension was selected for cross-sectioning. SEM imaging was performed as required during particle selection, milling, and lamella transfer. Images were acquired at an acceleration voltage of 3 kV using a secondary-electron detector, either an Everhart–Thornley detector or an in-column detector, and a working distance of approximately 4 mm.

Before cooling and ion-beam milling, the selected particle was coated with a protective platinum layer approximately 3–5 µm thick. This layer protected the active material during milling and provided improved contrast for locating the sample surface during subsequent TEM measurements. Initial milling was performed using a Ga^+ ion beam at 30 kV, with beam currents between 1 and 10 nA depending on the preparation stage. A lamella several micrometres thick was initially produced to maintain mechanical stability during lift-out.

The lamella was transferred to a Lacey Carbon Type-A copper TEM lift-out grid (Ted Pella, No. 01890) using an EasyLift micromanipulator. Because conventional FIB-induced material deposition is not feasible under cryogenic conditions, the lamella was attached to the micromanipulator and TEM grid by redeposition welding.

A final electron-transparent measurement window with lateral dimensions of approximately 2–5 µm and a thickness of approximately 100–200 nm was prepared by progressively reducing the ion-beam acceleration voltage and current. This gentle final thinning minimized ion-beam-induced damage to the sensitive structures. The final thickness was assessed from electron transparency at 2–3 kV and subsequently verified by monitoring the relative thickness, t/λ, during EELS acquisition.

Following preparation, the mounted lamella was returned to the argon-filled glovebox using the EM VCT100 system. It was then mounted on a cryogenic vacuum-transfer TEM holder for subsequent TEM, STEM, EELS, and EDS measurements under cryogenic conditions.

Cryo-TEM, STEM, EELS, and EDS Measurements

Cryo-TEM and STEM measurements were performed using a double spherical-aberration-corrected JEOL GrandARM microscope operated at 300 kV at ETH Zürich. The microscope was equipped with two large-area silicon drift detectors for EDS, each with an active area of 100 mm² and a combined solid angle of 1.6 sr. EELS measurements were performed using a Gatan 965 GIF Quantum ER imaging filter and spectrometer.

The sample was transferred using a MelBuild cryogenic vacuum-transfer holder and cooled to approximately −193 °C with liquid nitrogen. EDS and EELS data were analysed using Analysis Station (JEOL) and Gatan Microscopy Suite 3, respectively. Signal integrals were calculated within the corresponding software, and line-profile results were presented using a five-point moving average.

This preparation and characterization workflow minimized exposure to air and moisture and reduced alteration of sensitive reaction products during sample preparation and analysis. It therefore enabled structural and chemical information to be obtained with substantially fewer preparation-induced artefacts.

Electrochemical Measurements

All custom-built, coin-cell-type electrochemical cells were assembled under an inert atmosphere in an argon-filled glovebox. The cells consisted of an aluminium current collector 18 mm in diameter, a coated carbon/sulfur composite cathode, a polypropylene separator coated with ceramic on both sides and measuring 20 mm in diameter, and a lithium-metal anode measuring 18 mm in diameter and 110 µm in

thickness (FMC Lithium Corporation). The electrolyte-to-sulfur ratio was maintained at 20 µL mg_s^{-1} to ensure continuous wetting of the separator.

Electrochemical characterization was performed using BioLogic VMP3 or MPG2 potentiostats/galvanostats. Galvanostatic cycling, including capacity-retention measurements, was conducted between 0.5 and 3.0 V versus Li/Li^+ at a rate of C/10, except during the rate-performance experiments.

For the rate-capability measurements investigating the influence of ball milling and carbon-particle size, the cells first underwent a formation discharge at C/10. This was followed by five discharge–charge cycles at each applied rate. Similarly, in the experiments examining the effects of the charge and discharge rates separately, all cells were initially discharged and, where required, charged once at C/10 before the respective rate sequence was applied.

Galvanostatic intermittent titration technique (GITT) measurements were conducted by interrupting the applied current after every 100 mAh g_s^{-1} of transferred capacity. The cells were then allowed to relax at open-circuit voltage for 2 h. The time-dependent potential relaxation was evaluated to confirm that sufficient equilibration had been achieved while maintaining a practical experimental duration.

The open-circuit potential-relaxation curves were normalized, and characteristic relaxation time constants were approximated from the point corresponding to (1-1/e) of the normalized potential change during discharge and (1/e) during charge.

Results

WP4 – Advanced Structural Characterization of Sulfur Conversion and CEI Formation

In one of our recent works (C. Prehal et al., Nature Communications 2022), we highlighted the use of in-situ small angle neutron/X-ray scattering (in situ SAXS/SANS) and stochastic modelling to investigate structural changes at the nanoscale in complex materials systems like post-lithium-ion batteries. However, stochastic modelling for data analysis, specifically using plurigaussian random fields (PGRF), is computationally demanding. The interpretation of results derived from PGRF can be complex, indicating challenges to use in situ SAXS/SANS and stochastic modelling also for microporous carbons and carbonate electrolytes, as proposed in ALISA.

In response to the computational challenges posed by the PGRF method, we developed a data analysis algorithm based on a convolutional neural network (CNN). As illustrated in Figure 4a, the process begins with the PGRF parameters serving as an input for the CNN. The CNN then predicts a small angle scattering intensity curve. This predicted intensity is subsequently compared to the experimental data using a mean absolute error. The resulting error is then fed back into the Bayesian optimization algorithm, guiding its search for optimal parameters.

Figure 4b provides a visual comparison between the fitted curves and the experimental data, highlighting the accuracy and precision of our approach. The set of parameters associated with each fitted curve and how they evolve over time during cycling is shown in Figure 4c. Replacing the analytical model with our trained CNN, we achieve a speed up by three orders of magnitude with a typical fit taking 2.5 s with a CNN versus 42 min with the analytical model.

One of the primary advantages of utilizing machine learning-based optimization algorithms, such as Bayesian optimization or particle swarm used in our previous work, over conventional optimization methods is their robustness. They are less likely to get trapped in local minima, allowing for a more extensive exploration of the parameter space. This capability significantly reduces the need for initial assumptions that were previously necessary. Once these optimal parameters are determined, we can visualize a three-phased stochastic representation of our sample.

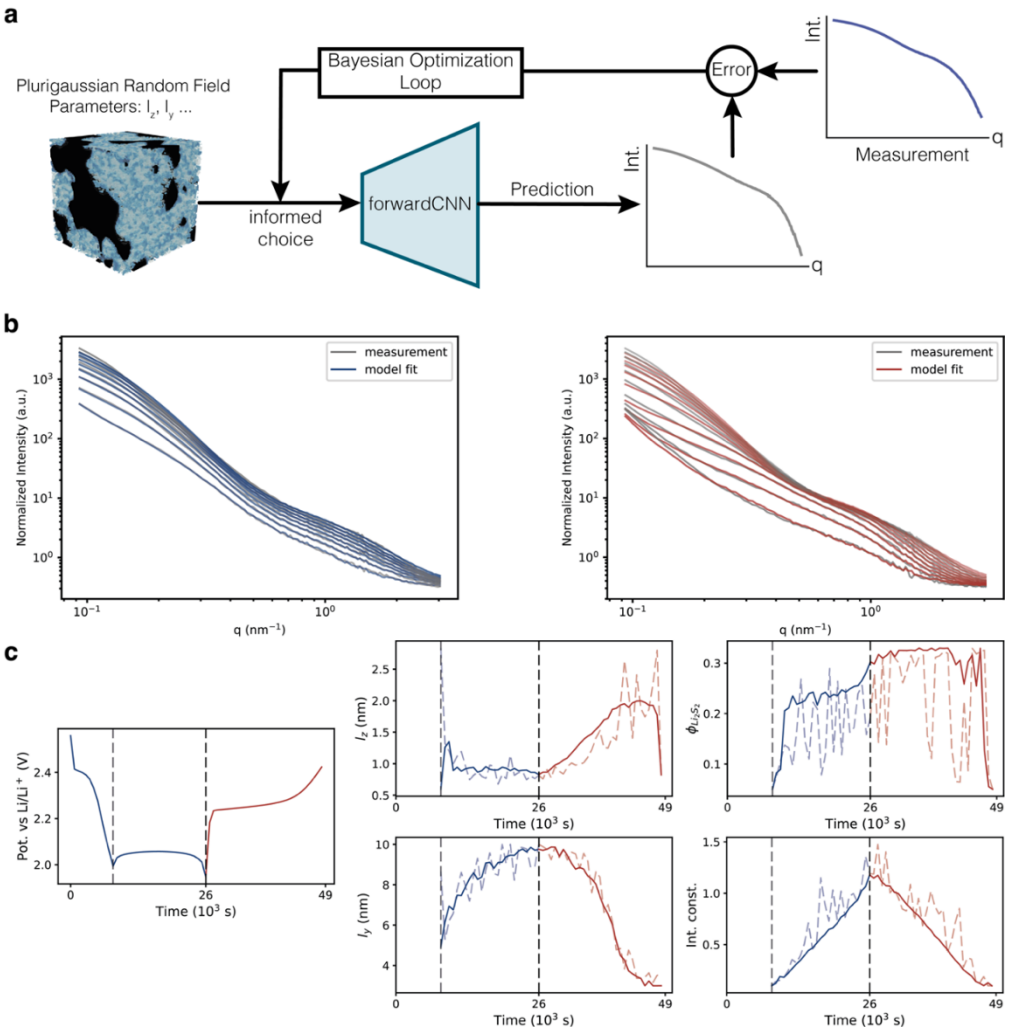


Figure 4 (a) Schematic representation of the fitting process. PGRF parameters are input into the CNN, predicting a small angle scattering intensity curve. The predicted intensity is then compared to experimental data using a mean absolute error, with the resulting error fed back into the Bayesian optimization algorithm. (b) Visual comparison of the fitted curves (blue = discharge, red = charge) against the experimental data, showcasing the accuracy and precision of the approach. (c) Evolution of the PGRF parameters over time during cycling.

While we have made significant strides in addressing the computational intensity of the PGRF method, the challenge of interpreting results remains. A key aspect of this challenge lies in the assumptions made regarding certain PGRF parameters. Often, these parameters are either held constant or confined within a selected range, which can introduce biases or uncertainties in the interpretation.

To provide a more grounded understanding and mitigate these challenges, we turned to Transmission Electron Microscopy (TEM) to examine discharged cathodes. TEM offers a detailed view of the structure, allowing us to discern correlations between phases and ascertain particle sizes. In Figure 5a, an overview of a carbon black agglomerate is presented. As shown in Figure 5b, a closer look reveals the discharge product adhering to the carbon black. Delving even deeper into the structure, Figure 5c displays that the larger particle is, in fact, an agglomeration of smaller lithium sulfide (Li_2S) crystals. The identification of Li_2S was confirmed by its distinctive crystal structure, which is evident in the Fast Fourier Transform (FFT) presented in Figure 5d.

While the micrographs underscore the potential of TEM in elucidating structural details, caution is essential when interpreting these images. The sample transfer from the argon-filled glove box to the TEM

was facilitated using a vacuum-transfer TEM holder. However, the material's inherent sensitivity to the electron beam meant that the sample underwent significant changes during observation. This highlights the necessity of cooling the sample to cryogenic temperatures to preserve its integrity during imaging.

To achieve this, we procured a cryo-vacuum transfer holder from Mel-Build (Japan). However, as detailed in section 2.2, the installation of this holder has faced delays, which has impacted our ability to obtain pristine, unaltered TEM images under cryogenic conditions.

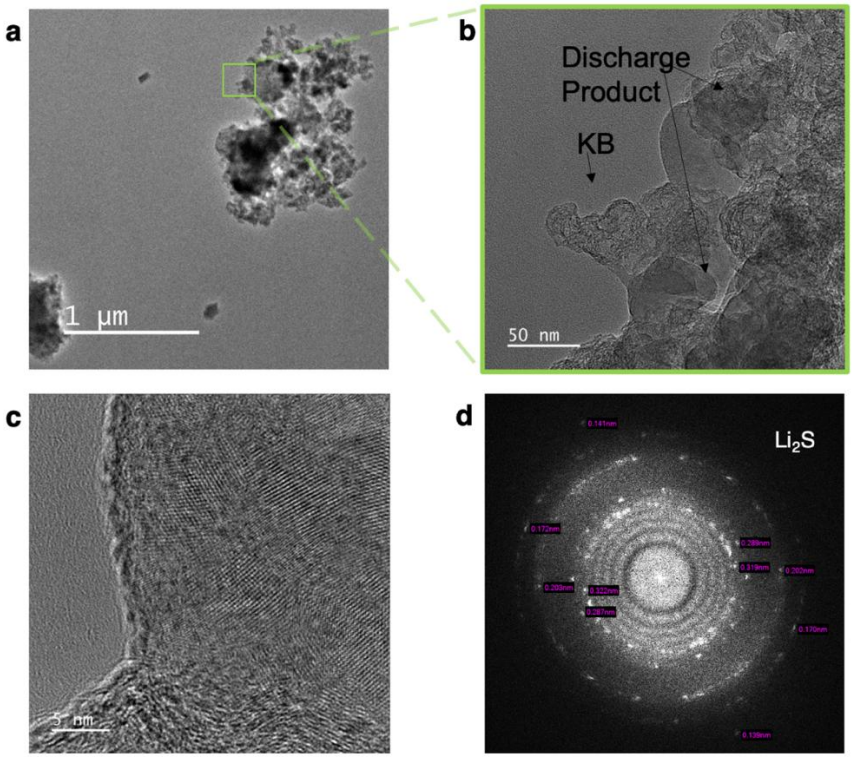


Figure 5: (a) Overview of a carbon black agglomerate from a discharged cathode, captured using Transmission Electron Microscopy (TEM); (b) Higher magnification TEM micrograph revealing the discharge product attached to the carbon black; (c) Further magnified view showing that the larger particle consists of smaller, aggregated crystals; and (d) FFT of the c clearly shows that the smaller crystals are lithium sulfide (Li_2S).

WP4 also has the goal to identify the structure-performance relationships on the nanoscale and derive design criteria for solid-state S-Li_2S conversion in microporous carbons. Therefore, we investigated the physicochemical mechanisms in microporous carbon-sulfur cathodes using *operando* X-ray diffraction (XRD), *operando* small angle neutron scattering (SANS) and various electrochemical characterization techniques include galvanostatic intermittent titration technique (GITT), electrochemical impedance spectroscopy (EIS). All these techniques could shed light on the poorly understood limiting mechanisms in this type of batteries. Systematically varied parameters like pore size and particle size of the microporous carbon host, sulfur loading in the composite cathode and the cycling rate would help to detect rate limiting factors in Li-S batteries and design the proper carbon for the cathode.

Structural changes during galvanostatic cycling were monitored via operando SANS and XRD. The measurements were completed with a AC08 (pore size 0.8 nm)-S 1-1 cathode. In Figure 6d,e,f the represented intensity changes during cycling are relevant to scattering length density (SLD) differences between carbon matrix, pore and conversion products. During the first discharge there is almost 4 times increase in the SANS intensity without any shape change in the scattering graph. That implies the formation of Li_2S and CEI components in the nanopores without changing the pore structure and would be

the direct evidence of CEI formation. No significant changes during further cycles refer to the stability of CEI and the S/Li_2S conversion that takes place in the pores.

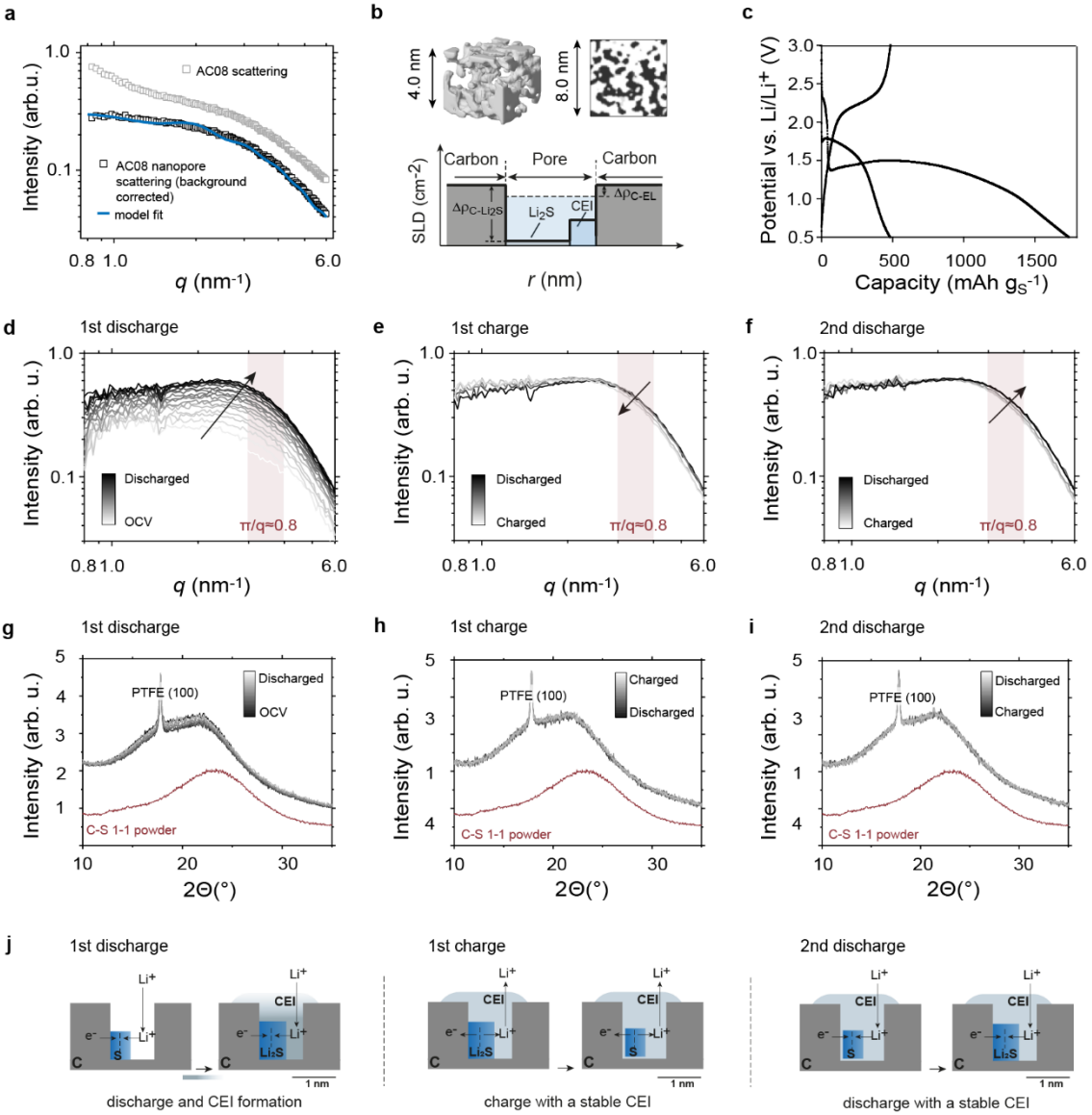


Figure 6: Operando SANS and XRD measurements. (a) Small angle X-ray scattering (SAXS) intensity of the AC08 carbon (grey) versus momentum transfer q, and after subtraction of the particle scattering at low q and the subtraction of a constant background (black). The blue solid line corresponds to a model fit based on Gaussian Random fields. (b) Top: 3D and 2D visualization of the AC08 nanopore structure based on the model fit in (a). Bottom: Sketch of scattering length densities (SLD) of different phases in the C-S composite. (c) Galvanostatic (dis)charge curves of the *in situ* SANS cell (AC08/S cathode with C/S ratio of 1/1). (d) SANS intensities versus scattering vector length q during first discharge. An increasing SLD difference (as shown in b) and the resulting SANS intensity increase indicate the CEI formation. (e) SANS intensities versus scattering length q during first charge. (f) SANS intensities versus scattering length q during 2nd discharge. *Operando* X-ray diffraction (XRD) intensity of an identical cell (AC08/S ration of 1/1) during (g) first discharge (h) first charge (i) second discharge. The absence of sharp crystalline S diffraction peaks during any cycling step confirms the solid-state conversion inside the nanopores. (j) Schematic summary of the processes occurring during 1st discharge, 1st charge, and 2nd discharge. The conversion takes place without causing any changes in nanopore structure and with no crystalline products.

The operando XRD measurements in Figure 6g,h,i confirm the conversion between S and Li_2S occuring in the pores. We know that orthorhombic S_8 crystals have distinct diffraction peaks, whereas the sulfur impregnated carbon only has a broad peak between 10 – 30° 2θ which is most likely related to amor-

phous S inside pores and in parts to the carbon. Also, the missing crystalline phases throughout cycling indicate that the discharge products and sulfur locate in the nanopores as amorphous phase.

In brief, the operando measurements helped to quantify the S/Li_2S and CEI structural evolution upon electrochemical cycling. In the following, we aimed to study the rate and capacity limiting factors in the Li-S batteries with solid state conversion in confinement. We consider there would be 2 main factors limiting performance, namely the Li-ion transport during the carbon particles and charge transfer between the active material and carbon (Figure 7).

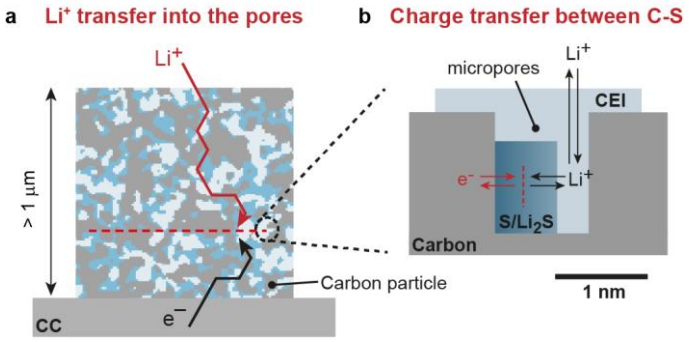


Figure 7: Possible rate and capacity limiting factors during solid-state conversion in confinement. Both Li ion diffusion into the carbon particle and charge transfer between carbon and active material could be rate limiting factors. The volume changes of sulfur during cycling might play a critical role.

During the electrochemical measurements we tested 2 activated carbons with different pore sizes of 0.8 and 1.2 nm and three different sulfur-to-carbon mass ratios of S/C=0.5, S/C=1 and S/C=2. The cells were cycled between 0.5-3V with a C/10 cycling rate. As shown in Figure 8, the electrochemical performance depends strongly on the pore size and S loading. The overpotential increases and the cells perform worse when the cathode consists of a carbon with larger pore size. Similarly, overpotential is larger when the fraction of sulfur is more than the amount that could be converted (e.g. S/C=2). Indeed, the capacity loading (capacity per geometrical cathode area) is highest for a S/C ratio of around 1/1, not around 2/1. This implies an optimum but not the highest S/C ratio must be achieved for the largest achievable capacity loading (mAh cm^{-2}) and longer capacity retention.

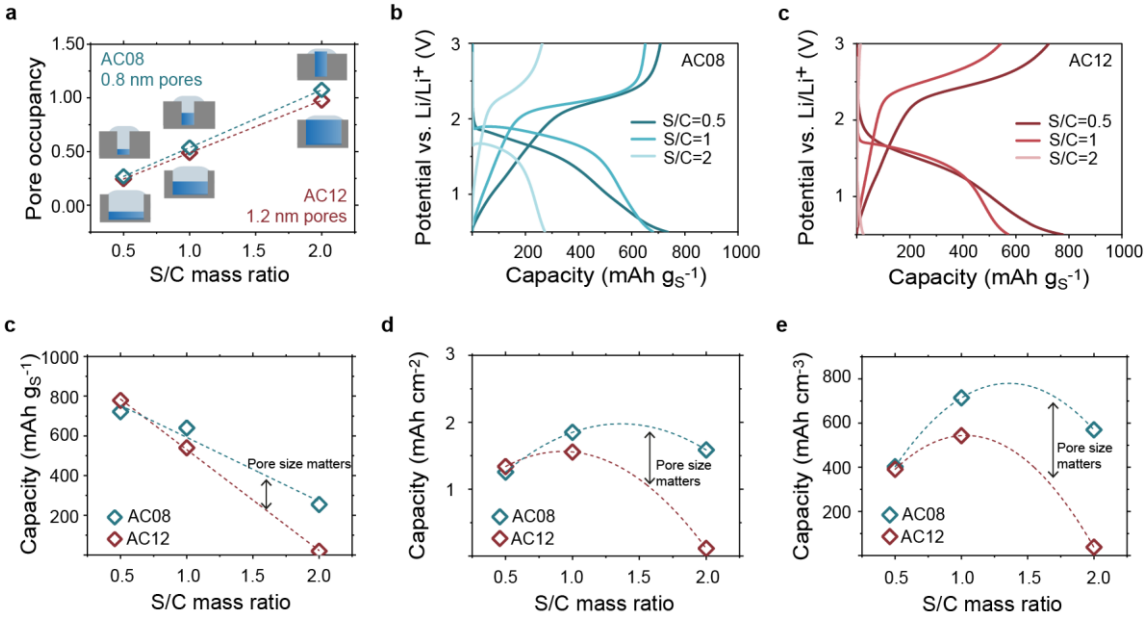


Figure 8: The effect of carbon pore size and sulfur loading on the electrochemical performance. (a) The theoretical pore occupancies as a function of S/C mass ratio. The dotted line serves as a guide to the eye to represent

the linear relation. Galvanostatic charge/discharge of AC08 (b) and AC12 (c) with different sulfur/carbon ratios (third cycle displayed). (d) Specific capacities (discharge at fifth cycle) as a function of the sulfur/carbon mass ratio. The dotted line (linear fit) serves as a guide to the eye. ed) The capacity loading in mAh cm^{-2} (discharge at fifth cycle) as a function of the sulfur to carbon mass ratio. The dotted curve (polynomial order of 2) serves as a guide to the eye. (f) The capacity loading in mAh cm^{-3} (per pore volume of pristine carbon based on GSA measurements (discharge capacity at fifth cycle) as a function of the sulfur to carbon mass ratio. The dotted curve (polynomial order of 2) serves as a guide to the eye.

The rate capability measurements were completed with discharging/charging rates of C/40, C/20, C/10, C/5, and C/2.5 for the two C-S composite cathodes (AC08 and AC12) and a C/S ratio of 1/1 (Figure 9). We find that a higher current density causes a larger overpotential, and a lower specific capacity, which means lower sulfur utilization. The maximum capacity is achieved with the slowest rate of C/40. Overall, the solid-state S/Li_2S conversion is slow; so capacities are strongly dependent on cycling rate. Also, the effect of pore size is clear during the rate capability test. With smaller pores (AC08), the cathodes have approximately 5 times larger capacity at the rate of C/5 compared to the cathodes with larger pores. This could be explained by the improved contact between sulfur and carbon and reduced charge transfer resistance in smaller pores. In the second part of the rate capability tests, we studied whether the charging of discharging is the rate-limiting step. The cells were constantly discharged with C/5 rate, the charging rate changed between C/20, C/10 and C/5. We observed that the discharge capacities followed the charge capacities, even though the cells were sometimes discharged 2-4 times faster. That suggests the discharge yield is controlled by the charging rate, since the oxidation reaction is relatively slow compared to the reduction reaction. We believe that volume changes in the active material during cycling affect the charge transfer resistance. During charging, the active material shrinks almost 80%, and that could hinder the charge transfer between the conductive carbon and active material (Figure 9d).

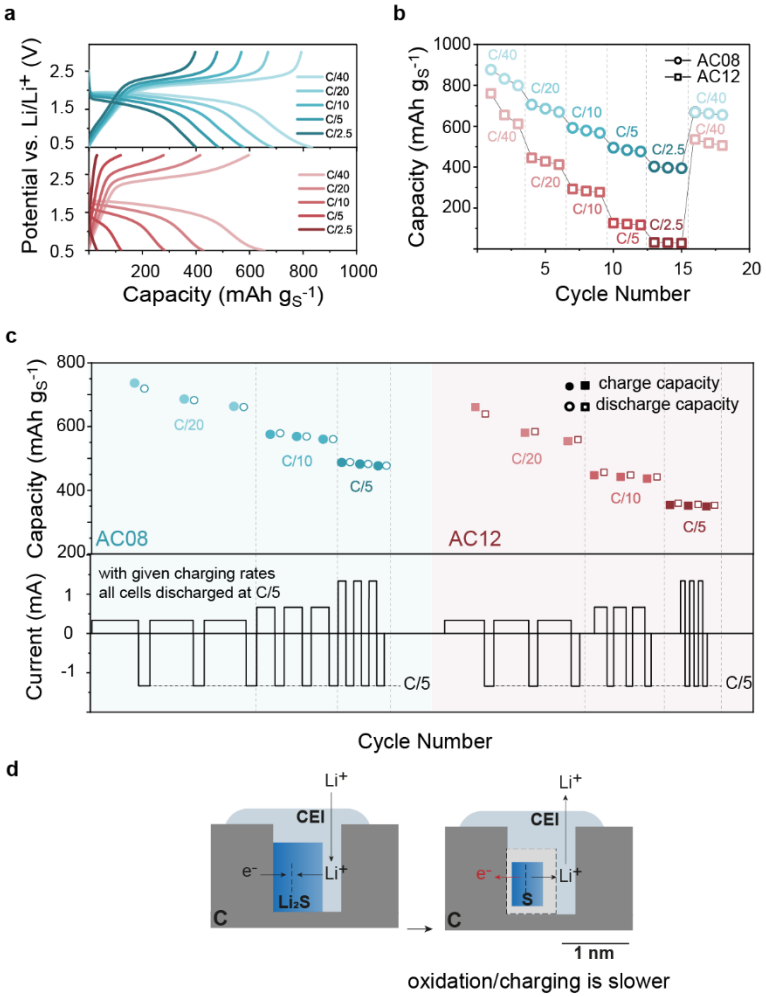


Figure 9: Rate capability data, based on gravimetric capacities. (a) Galvanostatic (dis)charge curves with different (dis)charge rates indicated as color tones. Blue and red represent the pore size of 0.8 nm (AC08) and 1.2 nm (AC12), respectively. The sulfur loading of the cathodes is 4.23 mgs (AC08) and 4.61 mgs (AC12). (b) Discharge capacities at different rates of C/40, C/20, C/10, C/5, and C/2.5. (c) Specific capacities for constant discharge rates but varying charge rates for AC08 and AC12. All cells are discharged with C/5, the charge rates are varied from C/20 to C/5. Filled shapes correspond to charging capacities, unfilled shapes correspond to discharge capacities. (d) Illustrative representation of conversion during cycling. Volume changes during cycling and especially shrinking during charging could be critical for rate limiting.

Our study suggests that the important factor for having a cell with good rate performances and long cycle life is the formation of a stable CEI. The experiments stressed the importance of the carbon nanopore structure on defining the stability of the CEI and cell capacities. All the performance studies where we vary the material and measurement parameters, suggested the carbon design strategies focusing on the pore size, pore size distribution and pore volume. We showed that the charge transfer between the active material and carbon is critical, and the contact should be maintained throughout cycling. Therefore, carbons with surface groups could help to have intimate contact. As another design parameter we should keep in mind that the carbon backbone should sustain the mechanical stress occurring due to the volume changes.

Our microscopy measurements aim to investigate the potential spatial distribution of CEI/active material during cycling. To map CEI components and discharge products, energy-dispersive X-ray spectroscopy (EDS) and electron energy loss spectroscopy (EELS) were performed under cryo-vacuum to avoid beam and air damage. Samples were prepared entirely under vacuum or cryo-vacuum to maintain structural integrity. After the first discharge, particles AC08 electrode were scratched onto carbon tape, and a large particle, chosen to highlight possible mass transport effects, was coated with platinum and milled in its center using cryo-FIB (Figure 10a, left). The resulting lamella, several microns thick, was mounted on a TEM grid (Figure 10a, middle) and further thinned to ~100–200 nm, with thickness verified by electron transparency and EELS t/λ values (Figure 10a, right).

Elemental mapping of fluorine was used to assess LiF content, since LiF is a common and stable CEI component in fluorinated electrolytes. The fluorine signal varied across particle depth, showing a clear enrichment near the surface, with significant concentrations confined to the outer ~1 µm (Figure 10d).

Cryo-EDS analysis of the cryo-FIB-prepared lamella shows a uniform sulfur distribution across the examined region (~2 µm depth), with no major variations in concentration. However, due to the elemental sensitivity limits of EDS, the exact origin of sulfur cannot be resolved, it may arise from discharge products, CEI species, or unreacted sulfur. To gain deeper insight into CEI formation, fluorine was chosen as a marker element. Lithium cannot be reliably detected by EDS, and most other CEI phases either contain sulfur or involve complex multi-elemental chemistries that hinder clear identification. In contrast, fluorine mapping provides a reliable indicator of LiF, a well-known, beam-stable CEI component with a simple chemical structure. The fluorine signal exhibits a depth-dependent distribution, becoming enriched near the surface and concentrated mainly within the outermost ~1 µm (Figure 10d).

To achieve higher resolution and chemical sensitivity, STEM-EELS was employed. Line-scan measurements (Figure 10e) confirmed the presence of LiF within ~50 nm of the surface, identified by its characteristic core-loss feature at 62–69 eV (Figure 10f). These results are consistent with the EDS-based inference that fluorine corresponds to LiF. Despite cryo-conditions, Li_2S was observed to degrade under the beam in STEM-EELS, similar to certain organic CEI phases. Importantly, unlike EDS, STEM-EELS also detected residual bulk sulfur at ~200 nm depth, based on its distinct core-loss signature (Figure 10f). This suggests incomplete sulfur conversion even close to the surface, though with weak intensity.

Figure 10f presents quantified LiF and sulfur profiles along a 300 nm line scan. To correct for thickness variations introduced during FIB milling, all signals were normalized by the t/λ (zero-loss) ratio, which is plotted on the secondary axis as a validation check. The results (Figure 10g) show an inverse correlation: LiF peaks within the first ~100 nm where sulfur is lowest, while sulfur concentration increases toward the interior, indicating unreacted sulfur accumulation. Beyond this region, both LiF and sulfur reach a plateau for ~200 nm, followed by a notable drop in LiF at ~300 nm depth. These opposing trends are consistent with CEI formation, where LiF arises from nucleophilic reactions between carbonates and

polysulfides, consuming sulfur similarly to Li_2S formation. Taken together, the EDS and EELS results demonstrate that CEI formation is not confined to a thin surface layer but extends into the particle interior with a compositional gradient, suggesting that CEI growth in larger particles may be diffusion limited.

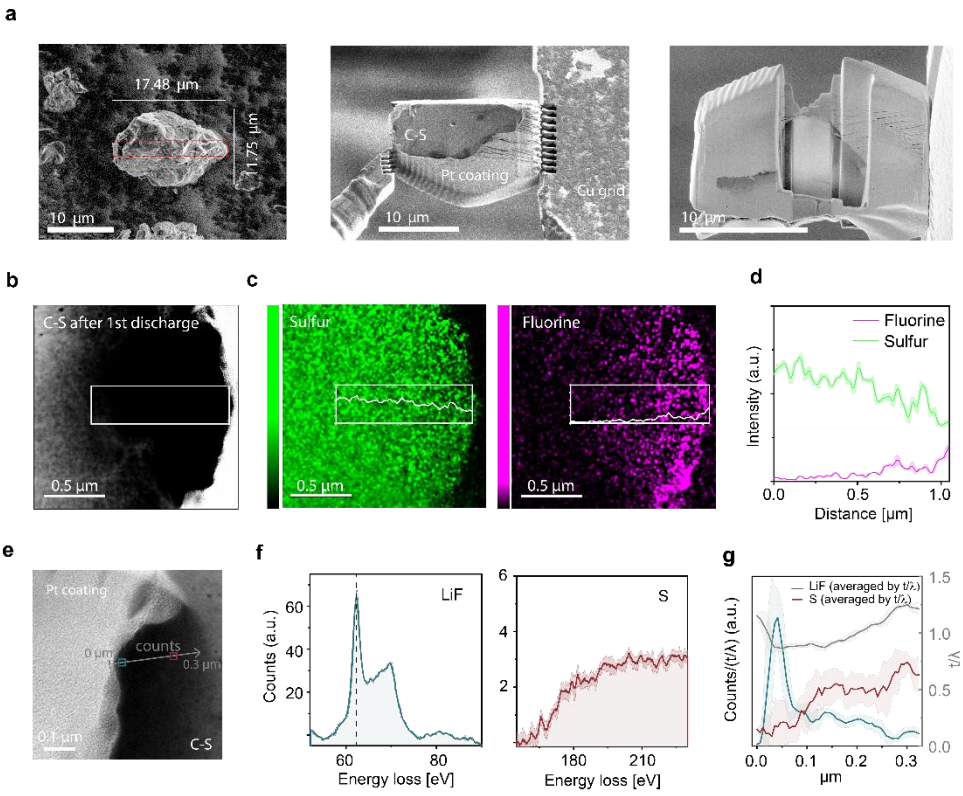


Figure 10: Lamella sample preparation, Energy Dispersive X-ray Spectroscopy (EDS) and Electron energy loss spectroscopy (EELS) results. (a) Lamella preparation for cryo-EDS and cryo-EELS: After the first discharge, material from a non-ball-milled carbon electrode was scratched onto carbon tape. A selected particle was coated with Pt, and a several-micron-thick lamella was extracted from its center using cryo-FIB SEM (red region in a-left). The lamella was transferred to a Cu TEM grid and thinned to 100–200 nm (right image). (b) STEM image of the lamella window, with the white-marked region used for quantitative EDS. (c) EDS elemental maps of sulfur (green) and fluorine (purple) show sulfur distributed into the particle interior, while fluorine is enriched near the surface. (d) Quantitative EDS confirms fluorine, likely from LiF, is concentrated within the outer ~1 µm of the particle. (e) TEM micrograph indicating EELS line-scan regions, with blue and red squares marking LiF and sulfur measurement sites, respectively. (f) EELS line-scan profiles of S (red) and LiF (blue) across 300 nm, with t/λ values (gray) validating data quality. LiF shows a strong peak within the first 100 nm, followed by an opposing trend with sulfur. (g) Left: energy-loss spectrum of LiF (~65–68 eV) at ~50 nm depth; Right: sulfur core-loss spectrum at ~200 nm depth (shoulder at ~160–165 eV), showing reduced sulfur intensity.

Ex situ cryo-TEM of discharged electrodes with 800 rpm ball-milled particles reveals heterogeneous CEI morphology. Contrast variations show that the CEI is not a uniform layer but a mix of organic and inorganic phases. The organic domains appear blob-like and beam-sensitive, while inorganic regions display clearer structural features. FFT analysis identified nanocrystalline phases corresponding to the (111) planes of LiF and Li_2S within the CEI (Figure 11 mid and bottom row). These results indicate a complex, electrochemically active surface that may drive parasitic reactions and capacity fading.

Microscopy reveals that CEI components are unevenly distributed within the particle volume, unlike sulfur which infiltrates uniformly during melt infusion. EDS confirms LiF, and thus CEI, extending ~1 µm below the surface. Since CEI phases conduct Li^+ but not electrons, while carbon provides electronic pathways, regions where sulfur, carbon, and CEI co-exist likely act as electrochemically active zones with enhanced transport and reaction kinetics. We define these regions as active material complexes, analogous to triple-phase boundaries (TPBs) known to govern electrochemical activity in solid-state Li–

S batteries. The CEI's complex nanostructure, with grain boundaries and interfaces, may further promote transport. The active regions are needed to facilitate superior electrochemical performance, therefore the distribution of CEI is important.

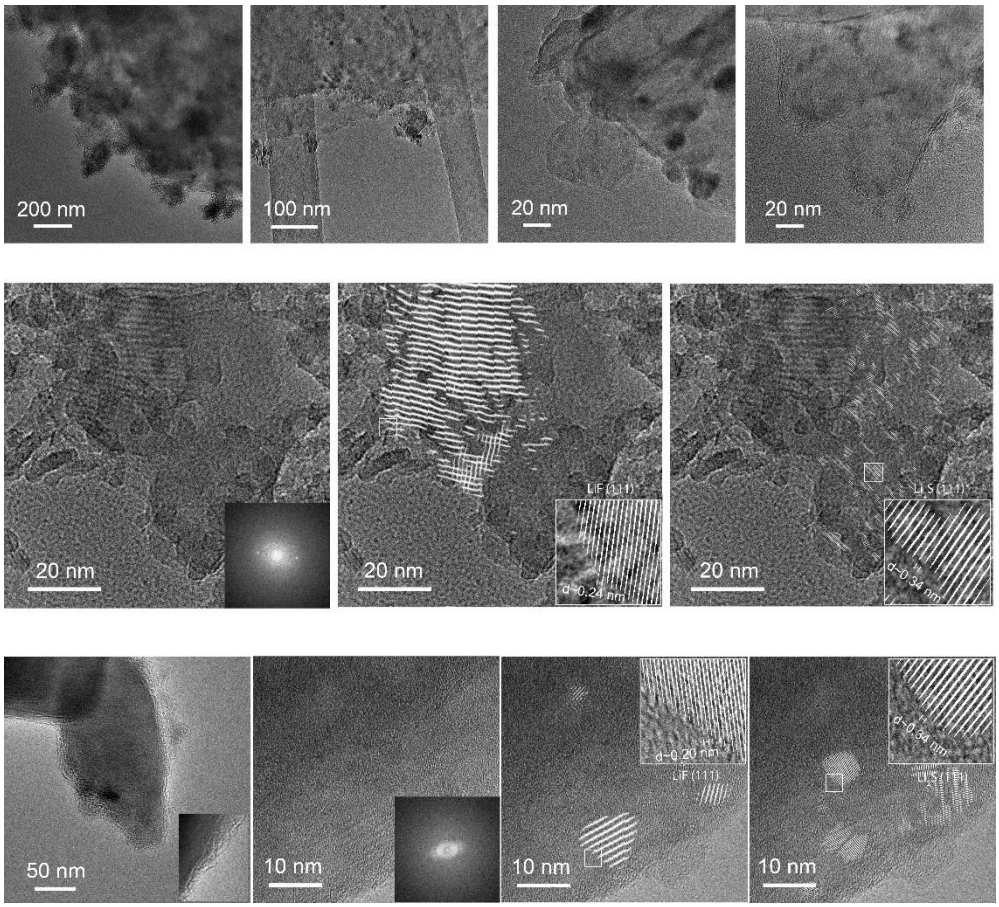


Figure 11: TEM analysis of 800 rpm ball-milled particles after first discharge. (a) TEM micrographs show a heterogeneous CEI comprising crystalline domains, solid clusters, and blob-like organic regions. (b) Crystalline Li_2S (111) and LiF (111) phases are identified on discharged particles, though binder residues are also visible due to electrode scratching. (c) When particles were directly discharged to eliminate binder effects, both Li_2S and LiF phases were again confirmed.

3 Conclusions and outlook

The ALISA project (Advanced Lithium–Sulfur Batteries with Ultramicroporous Carbons) developed and validated new carbon hosts, electrolyte formulations, and characterization methods for next-generation Li–S batteries. During the 36-month project period from September 2022 to August 2025, the consortium generated fundamental scientific knowledge, demonstrated new material concepts, and identified barriers to industrial implementation. The project therefore produced innovation-oriented results relevant to both Li–S battery research and future industrial development. The principal achievements are summarized below:

- **Carbon development (WP2):** An extensive portfolio of porous carbons was synthesized and optimized, including carbide-derived carbons (CDCs), novolac-derived carbons from the NPC

series, Porocarbs, carbon spherogels, and biomass-derived carbons such as olive-pomace-based CB700. Controlled pore sizes of 0.7–1.8 nm and tailored surface chemistry improved sulfur confinement and stability. Nitrogen and phosphorus functionalization provided additional surface properties that may also be relevant for applications such as catalysis and adsorption. The use of sustainable feedstocks for selected biocarbons further increased the environmental relevance of the developed materials.

- **Cathode engineering and electrolytes (WP3):** A standardized and reproducible sulfur-infiltration procedure was established. Systematic electrolyte benchmarking identified $LiPF_6$ in FEC with a high FEC content as the most stable carbonate-based formulation investigated, enabling reversible solid-state sulfur conversion. High-loading cathodes containing more than 50 wt% sulfur and based on NPC or Porocarb materials achieved capacities of up to 600 mAh g_s^{-1} for more than 50 cycles. Selected biocarbon cathodes retained approximately 850 mAh g_s^{-1} over more than 300 cycles. The standardized infiltration method and optimized electrolytes with fluorinated components provide transferable approaches for future laboratory-to-pilot-scale development. A pouch-cell prototype with a sulfur loading of 3.5 mg_s cm^{-2} was also fabricated, allowing initial scale-up strategies to be assessed and revealing key bottlenecks related to lithium-metal stability and electrolyte distribution.
- **Advanced structural characterization (WP4) (ETH):** *Operando* SAXS/SANS, XRD, XPS, and cryo-TEM provided detailed insights into sulfur-conversion mechanisms and interphase formation. SANS and XRD supported a solid-state sulfur-conversion mechanism within micropores and showed no evidence of crystalline polysulfide phases. XPS and cryo-TEM demonstrated that the composition and evolution of the cathode–electrolyte interphase (CEI) depended on the cell voltage and electrolyte chemistry. Carbonate-based electrolytes formed comparatively robust, inorganic-rich CEIs, whereas ether-based electrolytes produced less stable, polysulfide-rich interphases. A convolutional neural network model accelerated SAXS/SANS data analysis by approximately 1000 times, enabling rapid processing of complex datasets. This methodological advance is also potentially applicable to other nanostructured materials beyond battery research.

Overall, ALISA clarified the relationships between carbon structure, interfacial chemistry, sulfur conversion, and electrochemical performance. It identified promising development routes, including sustainable biocarbon hosts, functionalized porous carbons, standardized infiltration methods, and optimized carbonate electrolytes, while defining the remaining challenges for pouch-cell scale-up and lithium-metal operation.

The project also trained MSc, PhD, and postdoctoral researchers, strengthening the European knowledge base in post-lithium-ion energy storage. By delivering new materials, transferable methods, advanced analytical tools, and a prototype cell, ALISA established a basis for continued research and cost-effective innovation in the European energy-storage sector.

4 National and international cooperation

The consortium cooperated efficiently throughout the three-year project. Communication and collaboration were well structured and continuous.

Meetings: The project started with a kick-off online meeting on 15 September 2022. This was followed by the first face-to-face consortium meeting in Ljubljana (7–9 March 2023) and the second in Saarbrücken at INM (9 January 2024). In addition, an online consortium meeting took place in December 2024 to align reporting and finalize deliverables. A final consortium meeting was held online in June 2025 to conclude the project and review outcomes.

Cross-WP collaboration: Bilateral meetings and technical discussions between partners were frequently organized to address specific WP tasks (e.g. transfer of carbons from INM to NIC, exchange of

operando cells between ETHZ and NIC, discussion on Porocarb replacement after Heraeus' withdrawal). Communication channels included regular email exchanges, online calls, and joint data analysis sessions.

Management and coordination: NIC ensured timely coordination of deliverables and reports, while INM and ETHZ contributed proactively to cross-WP integration. After the withdrawal of Heraeus in early 2024, responsibilities were smoothly redistributed to INM without disruption of workflows, demonstrating strong adaptability of the consortium.

Overall cooperation: The consortium functioned in a highly collaborative manner, with transparent information exchange, efficient problem solving, and constructive engagement at all levels. The cooperative environment significantly contributed to the timely achievement of project objectives and strengthened long-term partnerships among the involved institutions.

5 Publications and other communications

Senol Gungor, A., von Mentlen, J.M., Ruthes, J.G.A., Garcia-Soriano, F.J., Drvaric Talian, S., Presser, V., Porcar, L., Vizintin, A., Wood, V. & Prehal, C.; Understanding rate and capacity limitations in Li-S batteries based on solid-state sulfur conversion in confinement, ACS Applied Materials & Interfaces, 2025, DOI 10.1021/acsami.4c13183

Tarimo, D.J., Garcia-Soriano, F.J., Vizintin, A., Prehal, C. & Presser, V., Performance of microporous carbon cathodes and impact of cathode/solid electrolyte interphase formation using carbonate and ether-based electrolytes in lithium-sulfur batteries, ACS Applied Energy Materials, 2025, DOI 10.1021/acsaem.5c01629

García-Soriano, F.J., Cometto, F., Raviolo, S., Slosar, T., Tchernychova, E., Genorio, B., Dominko, R., Bracamonte, M. V., Vizintin, A.; Biocarbon from olive pomace residue as a sulfur host for carbonate-based lithium-sulfur batteries; Communications Materials, 2025, DOI 10.1038/s43246-025-00846-8

von Mentlen, J.-M., Senol Güngör, A., Demuth, T., Belz, J., Plodinec, M., Dutta, P., Vizintin, A., Porcar, L., Volz, K., Wood, V., Prehal, C.; Unraveling Multiphase Conversion Pathways in Lithium–Sulfur Batteries through Cryo Transmission Electron Microscopy and Machine Learning-Assisted Operando Neutron Scattering, ACS Nano, 2025, DOI 10.1021/acsnano.5c00536

von Mentlen, J.-M., Fiedler, M., Neumayr, K., Dutta, P., Senol Gungor, A., Dörfler, S., Amenitsch, H., Zaubitzer, C., Althues, H., Wood, V., Prehal, C., Operando Scanning SAXS/WAXS Cell Design for Multi-Scale Analysis of All-Solid-State Battery Systems, Batteries & Supercaps, 2025, DOI 10.1002/batt.202500428

Gungor, A. S., von Mentlen, J. M., García-Soriano, F. J., Zaubitzer, C., Plodinec, M., Ruthes, J. G., ... & Prehal, C. (2026). Intraparticular Heterogeneity Limits Capacity in Lithium–Sulfur Batteries With Carbonate Electrolyte. Battery Energy, 5(3), e70111.

6 References

(1) Robinson, J. B. et al. 2021 roadmap on lithium sulfur batteries. J. Phys. Energy 3, 031501 (2021).

(2) Xu, W. et al. Lithium metal anodes for rechargeable batteries. Energy Env. Sci 7, 513–537 (2014).

(3) Yang, C., Li, P., Yu, J., Zhao, L.-D. & Kong, L. Approaching energy-dense and cost-effective lithium–sulfur batteries: From materials chemistry and price considerations. Energy 201, 117718 (2020).

(4) Chen, Y. et al. Advances in Lithium–Sulfur Batteries: From Academic Research to Commercial Viability. Adv. Mater. 33, 2003666 (2021).

(5) Zhao, M., Li, B.-Q., Zhang, X.-Q., Huang, J.-Q. & Zhang, Q. A Perspective toward Practical Lithium–Sulfur Batteries. ACS Cent. Sci. 6, 1095–1104 (2020).

(6) Zhou, G., Chen, H. & Cui, Y. Formulating energy density for designing practical lithium–sulfur batteries. Nat. Energy 7, 312–319 (2022).

(7) Dörfler, S. et al. Recent Progress and Emerging Application Areas for Lithium–Sulfur Battery Technology. Energy Technol. 9, 2000694 (2021).

(8) Ellerington, I. Faraday Report - High-Energy Battery Technologies. (2020).

(9) Betz, J. et al. Theoretical versus Practical Energy: A Plea for More Transparency in the Energy Calculation of Different Rechargeable Battery Systems. Adv. Energy Mater. 9, 1803170 (2019).

(10) Yari, S., Conde Reis, A., Pang, Q. & Safari, M. Performance benchmarking and analysis of lithium-sulfur batteries for next-generation cell design. Nat. Commun. 16, 5473 (2025).

(11) Dörfler, S. et al. Challenges and Key Parameters of Lithium-Sulfur Batteries on Pouch Cell Level. Joule 4, 539–554 (2020).

(12) Duffner, F. et al. Post-lithium-ion battery cell production and its compatibility with lithium-ion cell production infrastructure. Nat. Energy 6, 123–134 (2021).

7 Project progress (confidential)

The project deliverables are summarized in Table 1. In the table, “M” denotes the project month (e.g., M1 refers to month 1 and M36 to month 36). ETH Zürich contributed specifically to the periodic and final reports (D1.3), the chemical characterization of the cathode surface (D3.2), cryo-TEM and EELS characterization of cycled electrodes (D4.1), the investigation of CEI formation and solid-state sulfur conversion in ultramicroporous carbons (D4.2), and the identification of critical parameters linking structure, chemistry, and electrochemical performance (D4.3).

Table 1: Project deliverables.

No.	Deliverable title	Nature[1]	Dissemination level[2] / link to document	Scheduled date	Current date
D 1.1	Consortium agreement	Protocol	CO	M1	M1
D 1.2	Minutes of consortium meetings	Meeting	CO Zenodo record 7277349	M1-12-24-36	M1-12-24-36
D 1.3	Periodic and final reports	Report	CO Zenodo record 8328732 Zenodo record 13859546 Zenodo record 17045160	M12-24-36	M12-24-36
D 2.1	Report on graded-porous model carbons	Report	CO Zenodo record 13859560	M12	M24
D 2.2	Report on macroporous and micro-macro-porous carbon synthesis	Report	CO Zenodo record 13859560	M24	M24
D 2.3	Report surface tailoring and graphitization influence	Report	CO Zenodo record 17189305	M32	M32
D 2.4	Report on scaled synthesis of optimized carbon	Report	CO Zenodo record 17189305	M36	-

No.	Deliverable title	Nature[1]	Dissemination level[2] / link to document	Scheduled date	Current date
D 3.1	Report on electrochemical performance of novel carbonaceous materials and the performance of new electrolyte compositions	Report	CO Zenodo record 14759670	M27	M36
D 3.2	Report on chemical characterization of cathode surface	Report	CO Zenodo record 17043572	M33	M36
D 3.3	Report on the setup and performance of Li-S prototype cells	Report	CO Zenodo record 17043646	M36	M36
D 4.1	Report with cryo-TEM and EELS microscopic images, showing the chemical composition and the atomically resolved structure of discharged and charged electrodes.	Report	CO Zenodo record 17044407	M15	M15
D 4.2	Report on the CEI formation and the reversible solid-state sulfur conversion mechanism in the confinement of ultramicroporous carbons.	Report	CO Zenodo record 17044407	M21	M21
D 4.3	Report that summarizes the critical parameters controlling structure, chemistry and electrochemical performance	Report	CO Zenodo record 17044407	M27	M36
D 5.1	Webpage on project ALISA	Website	PU LinkedIn project page	M3	M5
D 5.2	Communication and Dissemination Plan	Protocol	CO Zenodo record 7859036	M5	M8
D 5.3	Data Management Plan	Protocol	CO Zenodo record 7859049	M6	M8
D 5.4	Exploitation and Business Plan	Protocol	CO Zenodo record 13739152	M20	M24

[1] *Nature of the deliverable, for example: Report, Paper, Book, Protocol, Prototype, Website, Database, Demonstrator, Meeting, or Workshop.*

[2] *Dissemination level: PU = Public; INT = Internal (restricted to project participants); RE = Restricted to a consortium-specified group; CO = Confidential, for consortium members only.*

The ALISA consortium identified the following specific objectives to achieve the main goals:

• Objective 1: Development and production of novel carbonaceous materials, namely ultramicroporous carbide-derived carbons and so-called Porocarb carbons (Heraeus) with tailored macroporosity and ultramicroporosity;

• Objective 2: Control of electrode processing and electrochemical characterization of Li-S batteries with SSC;

• Objective 3: Identification of design criteria for improved mass loadings of solid active materials and improved capacities based on advanced structural characterization;

• Objective 4: Optimization of the cathode electrolyte interphase (CEI) formation and degradation processes in Li-S batteries with SSC; and

• Objective 5: Development of a Li-S battery prototype with micro-/macroporous carbons.

Fulfilment of objectives

The project successfully achieved its overarching objective: to establish structure–performance correlations in Li–S batteries using advanced carbon hosts and carbonate electrolytes.

• Objective 1 was achieved through the development of a diverse portfolio of porous carbons, including CDC, novolac-derived carbons (NPC series), Porocarb, biomass-derived carbons, and carbon spherogels. Their porosity and surface chemistry were systematically tailored and validated.

• Objective 2 was fulfilled via optimization of sulfur infiltration techniques and electrode preparation, yielding cathodes with stable cycling and high sulfur loadings.

• Objective 3 was realized by applying advanced structural characterization (operando SAXS/SANS, XRD, XPS, cryo-TEM), which identified the design criteria for robust sulfur conversion at higher loadings. **(ETH major contribution)**

• Objective 4 was met by demonstrating that carbonate electrolytes, particularly $LiPF_6$/FEC:DMC formulations, promote stable CEI formation, while also clarifying the degradation pathways of unstable systems.

• Objective 5 was partially achieved: a Li–S pouch cell prototype with micro-/macroporous carbons was successfully assembled, but performance was limited by lithium instability and scale-up constraints. This outcome nevertheless provided valuable insights for future development.

In addition, dissemination, exploitation planning, and researcher training were successfully delivered, going beyond the original scope of objectives.

The project followed the work plan closely, with a few deviations:

• CDC synthesis delay (WP2): Certification issues delayed CDC production in year 1. This was mitigated by prioritizing novolac carbons and Porocarb activation until CDC synthesis resumed in year 2.

• Withdrawal of Heraeus (WP2 & WP5): In January 2024, Heraeus withdrew from the consortium. Tasks were successfully transferred to INM, with deliverables D2.3 and D2.4 merged into D2.1 and D2.2. An administrative annex was signed and continuity ensured.

Overall, the project fully met its scientific and technical objectives, provided additional impact in dissemination and training, and delivered new knowledge that extends beyond the original work plan.

8 Data management plan and open access/data/model strategy (confidential)

The ALISA consortium followed a structured Data Management Plan (D5.3) to ensure that all data generated during the project were handled according to the FAIR (Findable, Accessible, Interoperable, and Re-usable) principles. The consortium ensured that data generated within ALISA were managed responsibly, stored securely, and made broadly available to the research community. By depositing data in open repositories and linking them to publications, ALISA facilitated reuse and maximized the scientific and societal impact of the project outcomes.

Data generated and formats

The project produced large amounts of digital data (>1 TB), primarily from electrochemical, physicochemical, and imaging experiments. Data were collected as raw and processed files in commonly used

formats (e.g. .txt, .csv, .xls, .opj/.opju) depending on the instrument type. Both raw and curated data were stored to ensure reproducibility and transparency.

Making data FAIR

Findable: Persistent identifiers (DOIs) were assigned to datasets associated with publications and public deliverables. File naming conventions followed the paper or deliverable title, with figures/tables clearly documented.

Accessible: Data underlying publications and project reports were deposited on Zenodo and institutional repositories, with open access as the default. Sensitive or IPR-protected datasets were shared under request and with partner consent.

Interoperable: Standard, open formats were used whenever possible to allow data exchange across research groups. Metadata descriptions ensured compatibility with different disciplines (materials science, electrochemistry).

Reusable: Data were licensed for reuse with minimal restrictions, with embargoes applied only in cases of IPR or patenting. The consortium committed to keeping datasets reusable for at least five years after project completion.

Ethics and compliance

No sensitive personal data were collected. Ethical and legal considerations were respected, and data sharing followed the provisions of the consortium agreement and national guidelines